Vegetation pattern formation and community assembly under drying climate trends

Michel A. Ferré,[1] Induja Pavithran,[1] Bidesh K. Bera,[1] Hannes Uecker,[2] and Ehud Meron[1,3]
[1)]*The Swiss Institute for Dryland Environmental and Energy Research, BIDR, Ben-Gurion University of the Negev, Sede Boqer Campus, Israel*
[2)]*Institut für Mathematik, Universität Oldenburg, Oldenburg, Germany*
[3)]*Department of Physics, Ben-Gurion University of the Negev, Beer Sheva, Israel*

(Dated: 30 September 2024)

Drying trends driven by climate change and the water stress they entail threaten ecosystem functioning and the services they provide to humans. To get a better understanding of ecosystem response to drying trends, we study a mathematical model of plant communities that compete for water and light. We focus on two major responses to water stress: community shifts to stress-tolerant species and spatial self-organization in periodic vegetation patterns. We calculate community bifurcation diagrams of spatially uniform and spatially periodic communities and find that while a spatially uniform community shift from fast-growing to stress-tolerant species as precipitation decreases, a shift back to fast-growing species occurs when a Turing bifurcation is traversed and patterns form. We further find that the inherent spatial plasticity of vegetation patterns, in terms of *patch thinning* along any periodic solution branch and *patch dilution* in transitions to longer-wavelength patterns, buffers further changes in the community composition, despite the drying trend, and yet increases the resilience to droughts. Response trajectories superimposed on community Busse-balloons highlight the roles of the initial pattern wavelength and of the rate of the drying trend in shaping the buffering community dynamics. The significance of these results for dryland pastures and crop production are discussed.

Global warming and climate change are accompanied by drying trends worldwide due to decreased precipitation and increased evaporative demand[1,2]. Understanding the response of plant communities to these trends is crucial for mitigating losses of essential ecosystem services[3], such as pastures in drylands, which constitute 78% of the rangelands worldwide[4], and crop production[5]. Two common response mechanisms are spatial self-organization of plant communities in vegetation patterns[6,7] and community shifts to stress-tolerant species, which generally involve loss of productivity[5,8]. However, the complex interplay between these mechanisms has hardly been addressed[9]. In this work, we study a model for pattern-forming communities of plants that make different trade-offs between fast growth and tolerance to water stress. We find that the spatial plasticity of vegetation patterns during drying trends, in terms of variable vegetation patch size and number, buffers shift to stress-tolerant less-productive species without compromising resilience, thereby bearing positively on dryland pastures, agriculture, and food security.

I. INTRODUCTION

Ecosystem response to drying trends may involve multiple mechanisms operating at different levels of ecological organization[10]. At the single-plant level, phenotypic changes can occur, such as stomata closure to reduce water loss or growing deeper roots to reach moister soil layers[11–13]. At the many-plants population level, vegetation pattern formation can occur, involving partial plant mortality and increased water availability to the surviving plants[7,14]. At the many-populations community level, community reassembly involving shifts from fast-growing species to stress-tolerant species may occur[8,15]. These mechanisms are likely coupled as stress relaxation by one mechanism affects the driving forces of other mechanisms.

While the interplay between different response mechanisms has been addressed and studied[10], the consideration of vegetation patterning in this context has escaped attention despite its wide occurrence in drylands[16–18] and non-drylands as well[6,19]. Exceptions include studies of the interplay between vegetation patterning and phenotypic changes[20], and between vegetation patterning and community reassembly[9,21]. The significance of vegetation pattern formation in relation to its interplay with other response mechanisms lies in its high spatial plasticity. Vegetation patterns adapt to water stress by reducing vegetation patch size, keeping their number constant (patch thinning), and eliminating patches (patch dilution). These adaptation forms correspond to trajectories within the range of stable vegetation patterns of different wavelengths as precipitation decreases, the so-called "Busse Balloon"[22,23]. The trajectories assume stair-case forms where the horizontal parts correspond to patch thinning in patterns of a given wavelength and the vertical parts to patch dilution induced by crossing out the Busse-Balloon's boundaries and crossing back into stable longer-wavelength patterns[24]. This spatial plasticity may buffer changes in the composition and diversity of plant communities along the rainfall gradient, as it acts to relax water stress and preserve water availability despite the reduced rainfall, but this effect has hardly been studied[9].

In this paper, we use a plant-community model in one space dimension (1d) to unravel the complex bifurcation structure of community vegetation patterns of different wavelengths and study trajectories in the Busse Balloon of plant communities for drying trends of different rates. In doing so, we demonstrate the roles of patch thinning and patch dilution in buffering community composition and mitigating transitions

to less-productive stress-tolerant species while increasing the systems' resilience to droughts.

II. A MODEL FOR PATTERN-FORMING PLANT COMMUNITIES

We study a trait-based model for water-limited plant communities that captures pattern-forming feedback associated with increased overland-water flow toward denser vegetation patches[7]. The model has been introduced in length in an earlier study[9] and is briefly reviewed here.

We characterize the community using a trait-based approach, where the focus is not on plant species but rather on selected plant traits and functional groups of species that share the same trait values[9,25,26]. This approach is more geared toward questions of ecosystem functioning and performance under drying trends. We consider a community divided into N functional groups of plant species that make different tradeoffs between investment in shoot growth and investment in tolerating water stress. We quantify these tradeoffs through the values of a dimensionless trait parameter χ defined on the unit interval[25–27], so that $\chi = 0$ represents plants with highest investment in growth and lowest investment in tolerating water stress, while $\chi = 1$ represents the opposite extreme of plants with lowest investment in growth and highest investment in tolerance. The ith functional group, χ_i, $i = 1,2,...,N$, then represents plant species with χ values within the interval $\Delta\chi = 1/N$ that precedes $\chi_i = i\Delta\chi$. The community is quantified by N biomass variables, B_i ($i = 1,...,N$), where B_i represents the spatial density of the above-ground biomass (shoot) of all plant species within the ith functional group.

The model consists of a system of partial differential equations (PDEs) for the N biomass variables and two water variables, W and H, representing spatial densities of below-ground and above-ground water, respectively, all in units of kg/m^2. The system of PDEs reads:

$$\partial_t B_i = \Lambda_i W B_i - M_i B_i + D_B \partial_x^2 B_i + D_\chi \partial_\chi^2 B_i \,, \quad (1a)$$

$$\partial_t W = IH - LW - \Gamma W \sum_{j=1}^{N} B_j + D_W \partial_x^2 W \,, \quad (1b)$$

$$\partial_t H = P - IH + D_H \partial_x^2 H \,, \quad (1c)$$

where the second 'trait derivative', $\partial_\chi^2 B_i \equiv N^2(B_{i+1} - 2B_i + B_{i-1})$, represents mutations at a very small rate D_χ. In these equations the growth rate of the ith functional group, Λ_i, the infiltration rate of above-ground water into the soil, I, and the evaporation rate, L, are given by the expressions:

$$\Lambda_i = \frac{\Lambda_0 K_i}{\bar{B} + K_i} \,, \quad I = \frac{A(\bar{\bar{B}} + fQ)}{\bar{\bar{B}} + Q} \,, \quad L = \frac{L_0}{1 + R\bar{B}} \,, \quad (2)$$

where $\bar{B} = \sum_{j=1}^{N} B_j$ and $\bar{\bar{B}} = \sum_{j=1}^{N} Y_j B_j$. The expression for the growth rates, Λ_i, models growth attenuation due to shading, quantified by the parameters K_i, which stand for the capacity of functional groups to capture light. Thus, functional groups investing preferably in shoot growth have high K_i values and are less affected by shading. The expression for the infiltration rate, I, is higher in vegetation patches compared to bare soil, quantified by the dimensionless parameter $0 \le f \le 1$ and the parameter Q. Low f values ($f \ll 1$) represent highly differential infiltration and constitute an essential element in the pattern-forming feedback associated with overland water flow towards denser vegetation patches[7]. The specific contributions of different functional groups to the infiltration contrast are quantified by the parameters Y_i. Finally, the expression for the evaporation rate, L, describes reduced evaporation in vegetation patches due to shading. A list of all model parameters, their descriptions, units, and their values are given in Table 1.

We use the mortality parameters M_i to quantify tolerance to water stress, as lower M_i values allow for positive fitness and growth with lower values of soil-water content (see Eq. (1a)). The tradeoffs χ_i, $i = 1,...,N$ between investments in shoot growth and in tolerance to water stress are defined using the parameters K_i and M_i as follows:

$$\begin{aligned} K_i &= K_{max} + \chi_i (K_{min} - K_{max}) \,, \\ M_i &= M_{max} + \chi_i (M_{min} - M_{max}) \,. \end{aligned} \quad (3)$$

Thus, $\chi_1 = 0$ represents the limit (as $N \to \infty$) of a functional group (K_{max}, M_{max}) with highest investment in growth and lowest investment in tolerance (highest mortality), while $\chi_N = 1$ represents the functional group (K_{min}, M_{min}) with lowest investment in growth and highest investment in tolerance. This tradeoff is likely to affect the contributions, Y_i, of the various functional groups to the infiltration rate I as denser roots associated with lower-χ species (increased investment in shoot growth) make the soil more porous and increase the infiltration rate. We therefore assume the following form for Y_i:

$$Y_i = Y_{max} + \chi_i (Y_{min} - Y_{max}) \,. \quad (4)$$

We study the model using numerical continuation methods based on the software package pde2path[28], where, in the community model, the trait and real spaces were discretized using finite difference and finite element schemes, respectively. As a preparatory step for the community model (1), we also study single-species models with just one functional group χ_i in (1), for instance $\chi = 0$ (stress-tolerant) or $\chi = 1$ (fast-growing), and in particular compare their Busse balloons with that for the genuine community model (1). The numerical continuation of the Busse Balloon boundaries of the single-species model is calculated by bifurcation point continuation[28,29] of the bifurcation-point at which periodic solutions become stable due to the subcritical nature of the periodic branches. For the community model we use the stability information computed together with the patterned branches to plot (i.e., sample) the Busse balloon.

We further study the model by direct simulations. The one-dimensional spatial domain of length 150 [m] is discretized by 500 equally spaced points. In trait space, the community consists of 35 functional groups. For the study of time-dependent drying trends, two monotonically decreasing precipitation rates P are used; in the lower rate P is reduced by 0.1 mm/y every year, while in the higher rate P is reduced

TABLE I. Model paremeters, their descriptions, numerical values and units.

Parameter	Description	Value	Unit
Λ_0	Growth rate at zero biomass	10.0	$m^2/(kg \cdot y)$
Γ	Water uptake rate	8.0	$m^2/(kg \cdot y)$
f	Infiltration contrast ($f \ll 1$ – high contrast)	0.01	-
A	Maximal value of infiltration rate I	3000.0	y^{-1}
Q	Reference biomass at which $I \approx A/2$ for $f \ll 1$	12.0	kg/m^2
L_0	Evaporation rate in bare soil	200.0	y^{-1}
R	Evaporation reduction due to shading	0.7	m^2/kg
K_i	Capacity to capture light	variable	kg/m^2
K_{min}	Minimal capacity to capture light	6.7	kg/m^2
K_{max}	Maximal capacity to capture light	35.599	kg/m^2
M_i	Mortality rate	variable	y^{-1}
M_{min}	Minimal mortality rate	14.15	y^{-1}
M_{max}	Maximal mortality rate	22.515	y^{-1}
Y_i	Relative contribution to infiltration rate	variable	-
Y_{min}	Minimal contribution to infiltration rate	0.069	-
Y_{max}	Maximal contribution to infiltration rate	0.11463	-
P	Precipitation rate	variable	kg/(m$^2 \cdot y$) or mm/y
χ	Tradeoff parameter	[0,1]	-
N	Number of functional groups	35	-
D_B	Biomass dispersal rate	1.0	m^2/y
D_W	Soil-water diffusion coefficient	80.0	m^2/y
D_H	Overland-water diffusion coefficient	1800	m^2/y
D_χ	Trait diffusion rate	10^{-4}	y^{-1}

by 1 mm/y every year. The integration time step is set to $dt = 5 \times 10^{-3}$. Additionally, we introduced fluctuations to the overland water H with an amplitude of 1% of its value to reflect spatial heterogeneities. During the patch dilution process, the wavenumber of the patterns is computed by counting the number of patches of the biomass in space. In the simulations, when the biomass values go below 1×10^{-2} kg/m^2, it is considered bare soil, and the simulation stops.

In the following, we will often use the term "single species" when referring to a single functional group, although the latter may contain many species. This is because a functional group is modeled in our formalism by a single biomass variable, as a single species is often modeled.

III. SINGLE-SPECIES STATES

In order to study the response of pattern-forming plant communities to drying trends, we need to understand the bifurcation structure of community states along the rainfall gradient, using the precipitation rate P as the bifurcation parameter. It is instructive, however, to begin with bifurcation diagrams for single species that make highly different tradeoffs.

A spatially uniform population of a plant species can go through a Turing instability to periodic patterns as the precipitation rate P drops below a threshold P_T[7]. Figure 1 shows bifurcation diagrams for the fastest growing species, $\chi = 0$, and for the most tolerant species, $\chi = 1$. The instability is subcritical in general, implying the persistence of stable periodic patterns before their onset, that is, up to the saddle-node bifurcation point, $P_{high} > P_T$, where the most persistent pattern disappears. In the bistability range of uniform vegetation and periodic patterns, $P_T < P < P_{high}$, localized pattern solutions exist (not shown in Fig. 1), which snake back and forth between the uniform and patterned solution branches[30]. As P further decreases, additional periodic patterns with longer wavelengths appear[22,31]. These patterns persist to significantly lower P values than the (unstable) uniform state does before the longest-wavelength pattern disappears in a saddle-node bifurcation at P_{low}. In the low precipitation range of their existence, their solution branches assume isola-like forms; the two points at which the periodic solution branch connects to the (unstable) uniform solution branch are very close to one another.

A comparison of the periodic solution branches (PP) for the two extremal functional groups in Fig. 1a,b reveals several aspects by which stress-tolerant species ($\chi = 1$) differ from fast-growing species ($\chi = 0$): (1) The Turing bifurcation point P_T is shifted to a lower P. (2) The saddle-node bifurcation point P_{high} is also shifted to lower P. (3) The range of periodic patterns $P_{high} - P_{low}$ decreases. (4) The biomass density decreases. These differences can be understood as follows.

The lower P_T value for $\chi = 1$ in comparison to $\chi = 0$ is a consequence of the lower water stress that stress-tolerant species experience compared to fast-growing species, which weakens the driving force for vegetation patterning. The existence of stable vegetation patterns of the $\chi = 0$ species at higher precipitation rates compared to the $\chi = 1$ species, that is $P_{high}(\chi = 0) > P_{high}(\chi = 1)$, can be attributed to the higher biomass density of the fast-growing species and the corresponding sharper infiltration contrast between bare soil and

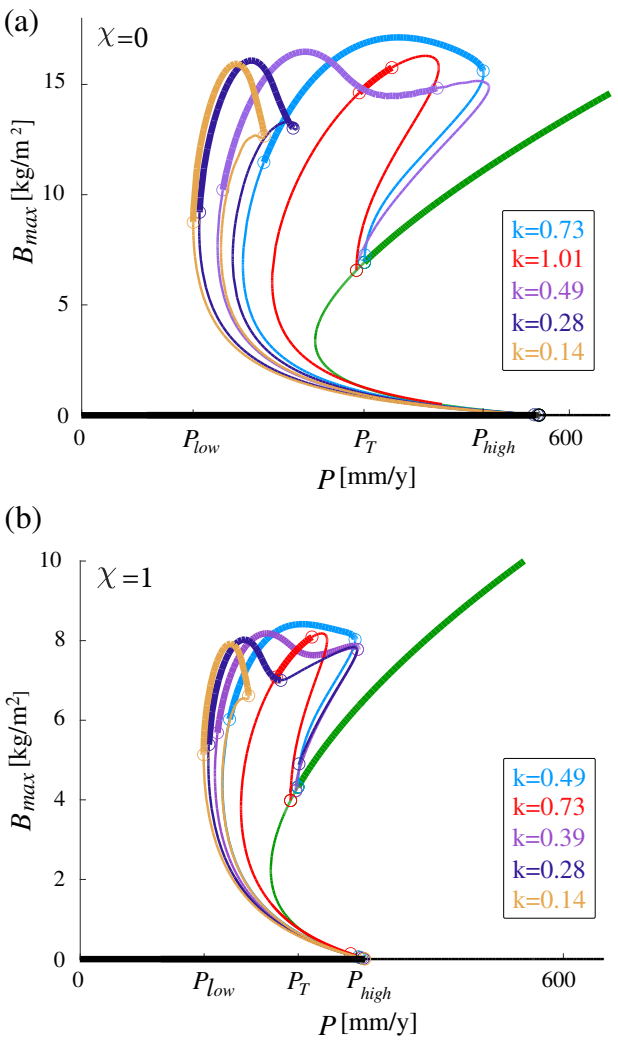

FIG. 1. Partial bifurcation diagrams of a single-species model for the extremal functional groups, $\chi = 0$ (a) and $\chi = 1$ (b). The vertical axis denotes the maximal value of the biomass density across the whole system. The black and green lines describe the bare-soil and uniform-community solutions, whereas the other colors describe periodic solutions of different wavenumber, as stated in the legends. Thick (thin) lines denote stable (unstable) solutions. The label P_T denotes the Turing bifurcation at which the uniform community becomes unstable to a patterned community (blue line). The labels P_{low} and P_{high} define the precipitation range where periodic patterns exist.

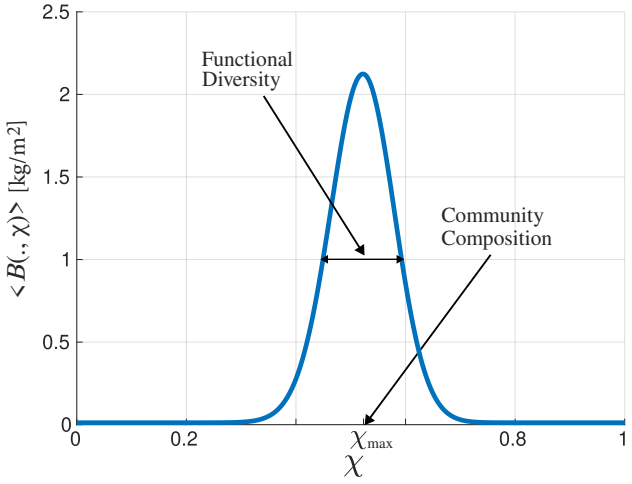

FIG. 2. Example of an asymptotic spatially averaged biomass distribution along the trait axis χ. The distribution contains information about community-level properties, such as the community composition χ_{max}, and the functional diversity quantified by the distribution width at half the maximal biomass density. The biomass distribution is calculated for $P = 418.9[mm/y]$.

vegetation patches that favors the onset of patterns[7]. The narrower range $P_{high} - P_{low}$ for $\chi = 1$ is a consequence of the small difference between the P_{low} values of the two species, which can be attributed to the existence of counter-acting processes. On one hand, stress-tolerant species should tolerate lower P values than fast-growing intolerant species. On the other hand, the higher biomass density in vegetation patches of the fast-growing species reduces soil-water evaporation and increases the amount of water plants can draw from their bare-soil surroundings because of a higher infiltration contrast. As a result, the water stress for fast-growing species is reduced. The lower productivity (smaller B) of the stress-tolerant species is a consequence of the inherent tradeoff between fast growth and stress tolerance.

A complementary view of the existence ranges of stable periodic patterns and their multi-stability is provided by the Busse balloons shown in Fig. 4[22,32]. The Busse balloon provides information about the wavenumber range of stable periodic patterns as a function of the precipitation. This range begins at $P = P_{high}$ and ends at $P = P_{low}$ (see Fig. 1). The wavenumber range at a given precipitation P provides information about the degree of multi-stability of periodic patterns at that precipitation value. Under conditions of drying climates, where the mean annual precipitation slowly decreases in time, the Busse balloon provides essential information about transitions to longer-wavelength patterns[24] and, thus, stress-relaxation by patch dilution.

IV. COMMUNITY STATES

The competition for water and light results in the emergence of a steady-state community, where only a subrange of the whole species pool, $0 < \chi \leq 1$, has practically non-zero biomass[9]. Figure 2 shows an example of a spatially uniform unimodal community, where the biomass is viewed as a continuous distribution in trait space, $B = B(\chi, x, t)$, with $B_i = B(\chi_i, x, t)$. Such solutions contain information about several community-level properties[9] including the community composition, measured by the most abundant trait, χ_{max} for which the biomass assumes its maximal value, B_{max}, and its functional diversity, measured by the width of the biomass distribution at $B_{max}/2$.

Drying trends are expected to shift the community composition to stress-tolerant species, but also to induce vegetation patterning, which may feedback on the community dynamics. Figure 3a shows a bifurcation diagram of asymptotic station-

ary community states, where the vertical axis is the χ value of the most abundant functional group, χ_{max}, obtained from a spatially averaged biomass distribution. The bifurcation parameter is the precipitation rate P. At high P, the uniform community state is stable and is dominated by fast-growing species (low χ). As precipitation decreases, a shift toward stress-tolerant species (higher χ) occurs, accompanied by a significant biomass decline, as the biomass distributions in the trait-space ($\chi - x$) plane $B(x,\chi)$ and the spatially averaged distributions $B(\chi)$ in Fig. 3a,b show. Below the precipitation threshold P_T, the uniform community state becomes unstable in a Turing bifurcation, and periodic community patterns appear with increasing wavelengths as P decreases further.

The emergence of periodic patterns is characterized by a significant decline of χ from the high value of the uniform community state that lost its stability to much lower values associated with the stable parts of the patterned solution branches. Ecologically, this decline represents a shift back to fast-growing species, as the bare-soil patches that form provide an additional water resource to the surviving plants, increasing the amount of water available to them.

The bifurcation diagram reveals another critical aspect of patterned communities – the low χ values they can support over a wide range of lower P values. This behavior is attributed to the high *spatial plasticity* of self-organized patterns, reflected here in two processes that involve partial plant mortality: (1) *Patch thinning* along each solution branch of a given wavelength, as the biomass distributions in the $\chi - x$ plane in Fig. 3c-e show. (2) *Patch dilution* by transitions to longer-wavelength patterns, as a comparison of the biomass distributions in Fig. 3e and 3f indicates. These processes maintain local water availability to the surviving plants, despite the drying trend, and thereby buffer changes in community composition over wide precipitation ranges.

The process of patch thinning is clearly visible by looking at the periodic solution that bifurcates from the uniform solution at P_T (blue line in Fig. 3) and at the biomass distributions in the $\chi - x$ plane shown in Fig. 3c-f; the number of patches does not change but each patch becomes thinner as P decreases. Patch thinning is effective in buffering community-composition changes in a relatively wide P range where χ_{max} hardly changes, as Fig. 3c,d shows, but at sufficiently lower P values it is no longer effective and a significant shift to higher χ values (stress-tolerant species) occurs (compare Fig. 3d and 3e). In this low P range, patch dilution by a transition to a longer-wavelength solution can relax the water stress and lower χ_{max}. These transitions occur as the boundaries of the community Busse balloon are crossed, as discussed in the next section.

The periodic patterns can be divided into two groups: solutions that connect to the uniform solution branch at distant bifurcation points and exist in the high P range (blue, magenta and red solution branches in Fig. 3), and solutions that connect to the uniform solution branch at nearly the same point, resembling isolas, and existing in the low P range (dark-blue and brown solution branches). Notably, the latter are characterized by pairs of equal χ values at different P values, as the circles f,g on the dark-blue solution branch and the corresponding $\chi - x$ biomass distributions in Fig. 3f,g indicate. The higher biomass at the higher P value (Fig. 3f) implies stronger uptake of soil water compared to the uptake at the lower P value where the biomass is lower (Fig. 3g). The combined effect of higher P and stronger water uptake can result in equal levels of water stress at different P values and, thus, equal χ values.

In the bistability precipitation range of uniform-vegetation and patterned solutions a subrange of homoclinic-snaking exists[33], characterized by a high multiplicity of stable localized patterns of different size. These localized patterns appear in the bifurcation diagram shown in Fig. 3 as solution branches (turquoise lines) that snake back and forth between the uniform solution branch (green line) and one of the periodic solution branches (magenta line). The uppermost (highest χ_{max}) solution branch describes a spatially uniform community with a single gap of bare soil (Fig. 3h), whereas the downmost solution branch describes a community gap pattern with a single missing gap (Fig. 3j). The solution branches in between describe patterned domains in otherwise uniform community or uniform domains in otherwise patterned community (Fig. 3i), where branches with lower χ_{max} correspond to larger patterned domains, where faster-growing species reside. The localized patterns give rise to significantly wider functional diversity as they contain two distinct niches: a uniform niche for more stress-tolerant species and a patterned niche for faster-growing species. This effect can be stronger with different parameter settings, and may lead not only to widened unimodal $B(\chi)$ distributions, but also to bimodal distributions[9].

Spatial patterning and community assembly mutually affect each other; a community shift to stress-tolerant species delays the onset of Turing patterns to a lower precipitation rate, and the onset of patterns shifts the community back to fast-growing species and buffers further community changes. A comparison between the Busse balloons of a single species and of a community uncovers additional aspects of these mutual relations. As Fig. 4 shows, the community's Busse balloon occupies intermediate ranges in the (k,P) plane in comparison to the ranges of $\chi = 0$ and $\chi = 1$. The prominent differences are in the high P range; the $\chi = 0$ Busse balloon extends to significantly higher P and k values than the community Busse balloon, while the opposite holds for the $\chi = 1$ Busse balloon. This can be attributed to the stronger pattern-forming feedback associated with the fastest-growing species $\chi = 0$, which form highly dense vegetation patches and strong infiltration contrasts. The resulting stronger pattern-forming feedback extends the stability range of periodic patterns to higher P values. Interestingly, the community Busse balloon extends beyond the Busse balloon of the stress-tolerant species also at low P. This can be attributed to a community facilitation effect, where faster-growing species in the community increase the infiltration rate in vegetation patches and, thereby, the overland water flow toward these patches from which all species benefit.

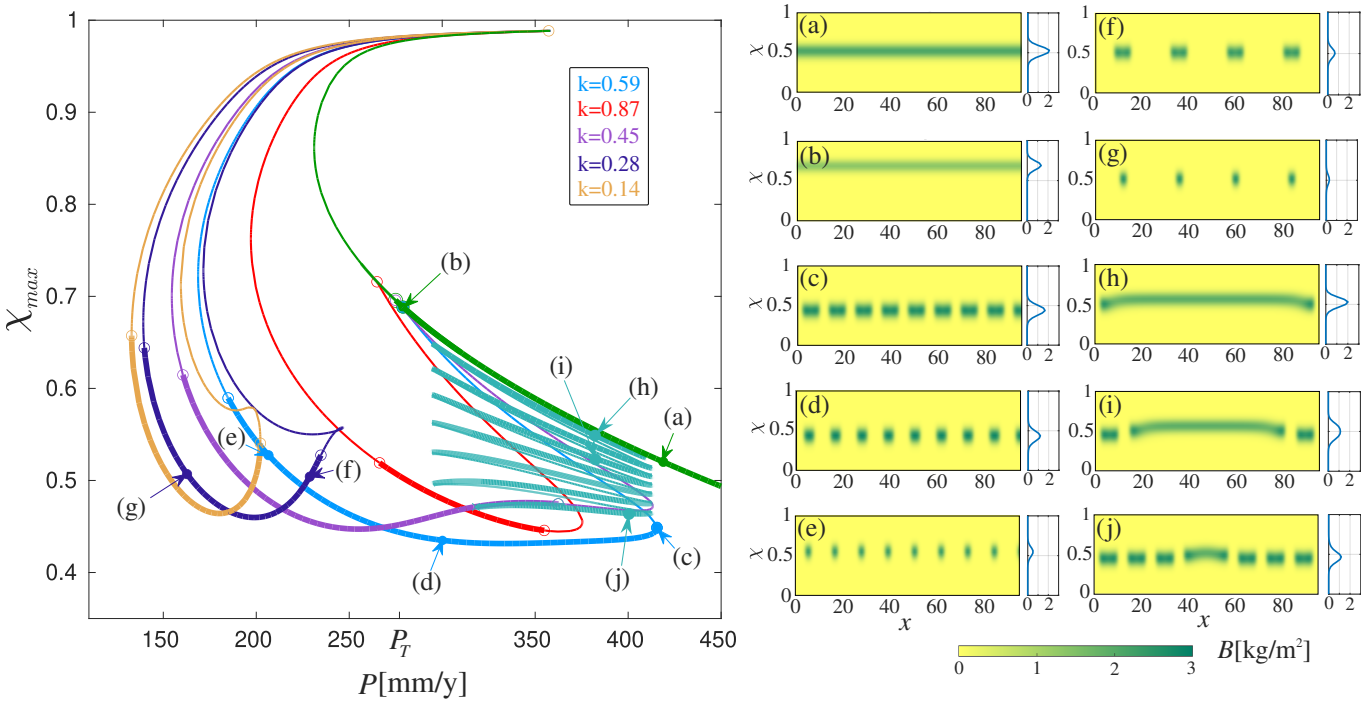

FIG. 3. A community bifurcation diagram. Shown are solution branches (left) and examples of the corresponding biomass distributions (right). The green solution branch describes a spatially uniform community, which loses stability in a Turing bifurcation at P_T. Panels (a,b) show the shift to stress-tolerant species as P decreases. The turquoise solution branches that snake back and forth describe localized patterned domains in otherwise uniform communities. Panels (h-j) show examples of such localized patterns. The other colored solution branches represent patterned communities with wavenumbers decreasing as as stated in the legend. Panels (c-e) demonstrate patch thinning. Panels (f,g) show different precipitation rates that give rise to the same community composition χ_{max} albeit different biomass densities. Thick (thin) lines denote stable (unstable) solutions. Hollow circles denote bifurcation points. Solid circles refer to the biomass distributions shown in panels (a-j), which were calculated at the corresponding precipitation rates.

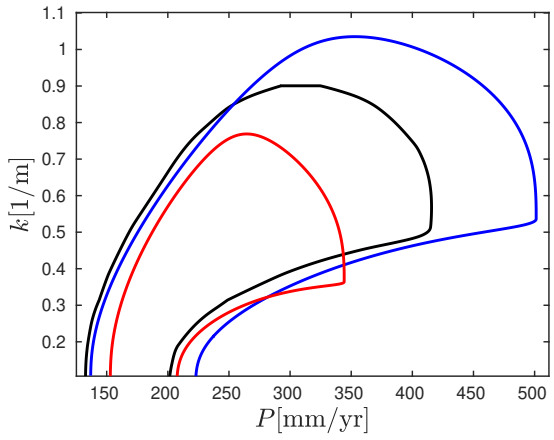

FIG. 4. Single-species vs. community Busse balloons. Shown are Busse balloons, depicting the ranges of stable periodic patterns in the precipitation-wavenumber ($P-k$) plane, for the extreme functional groups $\chi=0$ (blue line) and $\chi=1$ (red line) and for the community (black line). Notice that the Busse-balloon boundaries do not extend to $k=0$ because of the finite system size used in the calculations.

V. RESPONSES TO DRYING TRENDS OF INCREASING RATES

The bifurcation diagram shown in Fig. 3 provides information about the community response to an infinitely slow drying trend in the course of which the community closely follows the stable parts of the solution branches. The community's Busse balloon provides additional information; depending on the wavenumber of the initial pattern, different mixes of patch thinning and patch dilution may occur. Figure 5 shows community trajectories, superimposed on the Busse balloon, starting from different initial wavenumbers and responding to drying trends of different rates. The drying trends correspond to decreasing precipitation P at rates of 0.1mm/y and 1mm/y every year. A horizontal trajectory part of a constant wavenumber k, corresponds to a patch-thinning phase where the number of vegetation patches remains constant, but their size decreases. When the trajectory crosses the low-P boundary of the Busse balloon, the periodic pattern loses its stability, and a transition toward a stable pattern of lower wavenumber thereafter occurs. This transition is described by a vertical trajectory part and corresponds to patch-dilution events where the number of vegetation patches is reduced. In practice, the time span between patch-dilution events is often too short for the convergence to strictly periodic patterns. In these cases, the wavenumber value is determined by counting the number

of patches. To expedite the transitions to longer-wavelength patterns a weak heterogeneity in H is introduced.

Three initial wavenumbers are studied, representing narrower precipitation ranges of stable solutions as the wavenumber increases. As Fig. 5 shows, the mix of the two stress-relaxation modes, patch thinning and patch dilution, changes with the initial wavenumber; the higher the wavenumber, the shorter the first patch-thinning phase, and the larger the number of patch-dilution events. A lower initial wavenumber at high precipitation implies bigger patches and more room for patch thinning as the precipitation decreases. Indeed, the lowest initial wavenumber (Fig. 5a) gives rise to the longest patch-thinning phase before the Busse-balloon boundary is crossed. For most of this phase, the community composition χ_{max} (encoded by the color) comprises fast-growing species and hardly changes, but as the Busse-balloon boundary is approached, a sharp shift to stress-tolerant species occurs. By contrast, the patch-thinning phase for the highest initial wavenumber (Fig. 5c) is the shortest and the number of patch-dilution events is the largest. An intermediate case is shown in Fig. 5b. Thus, as the initial wavenumber increases, the time span of patch thinning decreases, and the number of patch-dilution events increases. This change in the mixture of the two stress-relaxation modes results in communities of faster-growing species in the relatively low precipitation range; shifts to stress-tolerant species by patch thinning are weaker, and stress relaxation by multi-patch-dilution events is stronger, favoring faster-growing species.

In the range of very low precipitation, all trajectories, irrespective of the initial wavenumber, culminate in highly stress-tolerant species before collapsing to bare soil occurs. In this range, the pattern wavelength becomes too long for patch thinning and patch dilution to be effective in retaining water availability as the drying trend continues, as the inter-patch distance exceeds the typical length of overland water flow before complete water infiltration into the soil occurs. The factors that affect this length, denoted here by d, can be assessed using dimensional analysis[34]: $d \sim \sqrt{D_H/A} \cdot g(QA/P)$, where g is an unknown function. According to this result d scales like $D_H^{1/2}$ and like $A^{-1/2}$ in cases where the function g approaches a constant asymptotic value. This is often the case when its dimensionless argument QA/P is either a very small or a very large number. In the present case, it is pretty large, of order $10^2 \gg 1$.

The effect of a ten-fold faster trying trend is shown in Fig. 5d-f for increasing initial wavenumbers. Since the low precipitation Busse-balloon boundary is now reached faster, the time span for community reassembly is shorter and patch dilution events occur for faster-growing species. This results in more moderate shifts to stress-tolerant species.

VI. DISCUSSION

Vegetation patterning involves partial plant mortality and soil-water redistribution and is therefore inherently related to the assembly and dynamics of plant communities under conditions of water stress. Our model studies suggest the existence of two phases in the response of plant communities to decreasing precipitation. The first phase occurs when the community is still spatially uniform and experiences a shift from fast-growing to stress-tolerant species. This shift delays the onset of patterns to lower precipitation rates. The second phase begins with the onset of vegetation patterns at the Turing instability threshold P_T. It involves a shift back to fast-growing species followed by a wide precipitation range (or time span) where the community composition hardly changes. This behavior is attributed to the high spatial plasticity of vegetation patterns, reflected in patch thinning along any solution branch describing a periodic pattern, and in patch dilution when transitions to patterns of longer wavelengths occur. Both processes involve partial plant mortality and act to increase water availability to the surviving plants, which compensates for the reduction in precipitation as the drying trend proceeds. As a consequence, they buffer community composition changes.

We focused on vegetation pattern formation in 1d systems, but the results are also applicable to vegetation bands in sloped 2d terrains, where 1d behaviors, such as the Busse balloon, have been observed[23]. Flat 2d terrains differ from 1d systems in that they allow for morphological changes. At the Turing instability hexagonal gap patterns typically emerge, and as precipitation further decreases, morphological changes to labyrinthine stripe patterns and hexagonal spot patterns occur, rather than transitions to longer-wavelength patterns[7]. However, the general principle of spatial plasticity buffering community changes still apply; the morphological changes gradually increase the bare-soil areas around vegetation patches and thereby increase the availability of water to the surviving plants, compensating for the reduction in precipitation.

For simplicity, we chose to analyze a model with a single dominant water transport mechanism – overland water flow, but the same bifurcation structure and spatial plasticity are realized with other mechanisms as well[35], either alone or in concert[36]. We therefore expect the main conclusions to be independent of the particular water-transport mechanism.

Our results bear on agriculture and food security, as in that context, the shift to stress-tolerant species may imply loss of crop productivity. This is because of the inherent tradeoff between growth and tolerance[5,8], and the consequent displacement of fast-growing crops by stress-tolerant species as a drier climate develops. The latter may not be edible, but even if they are, their productivity is low. Attempts at increasing crop productivity are currently made by means of genetic intervention, but so far with limited success[37,38]. Here, we point toward a conceptually different approach to this problem that, in addition to plant-level mechanisms, also considers a robust population-level mechanism, namely, self-organization in spatial patterns[27]. The onset of spatial patterns counteracts the shift to less-productive stress-tolerant species without compromising tolerance to water stress, as it provides an additional soil-water resource – the water plants draw from their bare-soil surroundings.

The interplay between spatial patterning and community dynamics may have significant implications for managing ecosystems under conditions of drying climates. Spatial patterning can be favored by introducing weak spatial periodic-

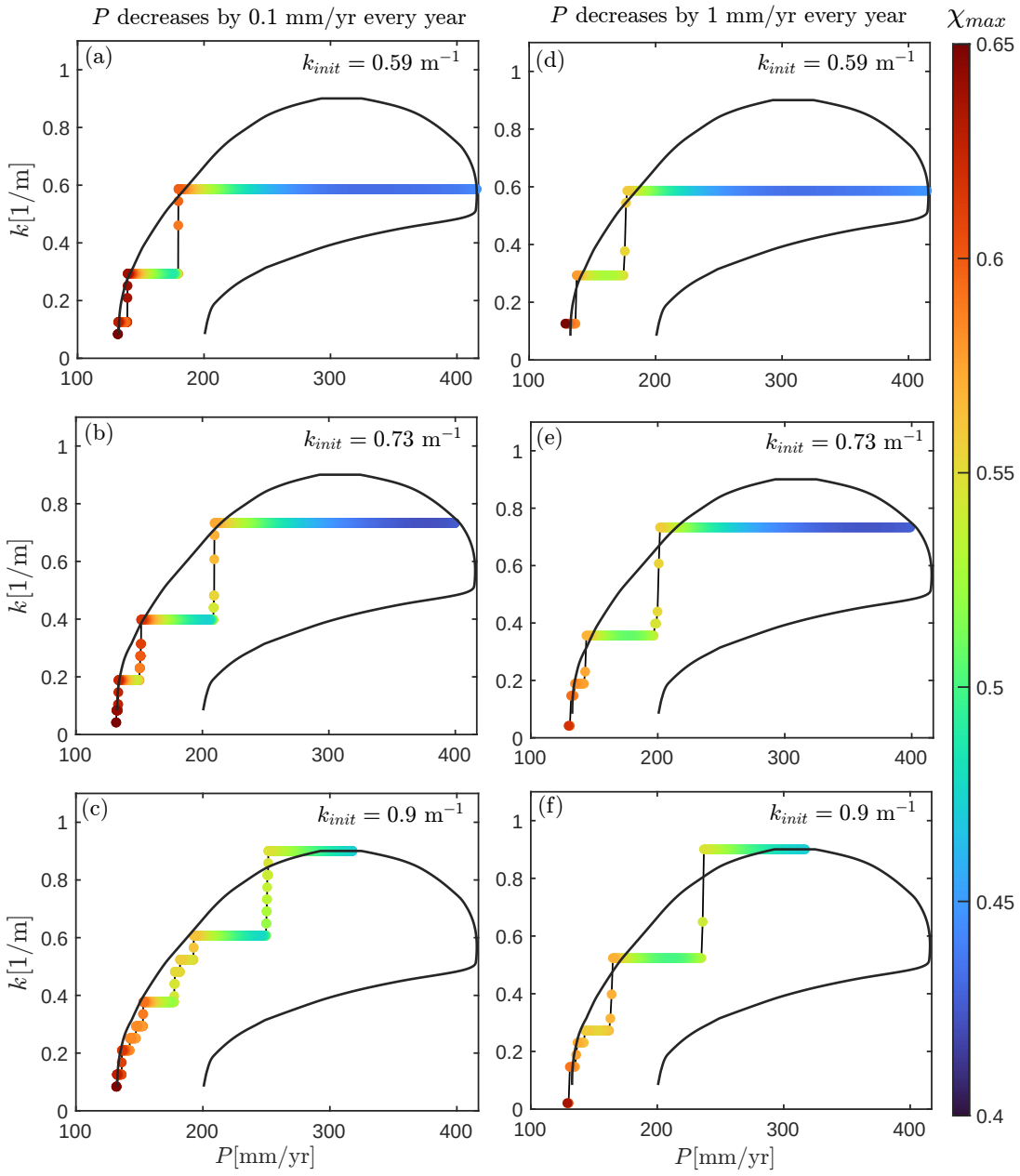

FIG. 5. Community trajectories, superimposed on the Busse balloon. Shown are trajectories emanating from initial patterns of increasing initial wavenumbers k_{Init} at two rates of precipitation decrease, slow (a-d) and fast (d-f) as indicated in the figure. The changing colors of the trajectories denote community composition changes according to the color bar on the right. Horizontal trajectory parts correspond to patch thinning wheres vertical trajectory parts correspond to patch dilution. Patch dilution events are triggered when the trajectories cross the lower-P boundary of the Busse balloon and the corresponding pattern becomes unstable.

ity under benign conditions when the vegetation is still uniform, to facilitate transitions to vegetation patterns of desired wavenumbers in the bistability range of uniform and patterned vegetation, and even below it[39]. Practices for that purpose may integrate provisioning ecosystem services, such as the provision of fodder for livestock, by non-uniform vegetation clear-cutting. Under conditions of mild stress, when vegetation patterns already exist, such practices can be used to favor particular wavenumbers, e.g. to obtain a strong community-buffering effect by patch thinning, or to introduce mixed vegetation states, uniform and patterned or patterned states of different wavenumbers, to create different niches and thereby increase functional diversity.

ACKNOWLEDGMENTS

This research has received funding from the Israel Science Foundation under grant No. 2167/21, and from the Euro-

pean Union's Horizon Europe – European Research Council programme under ERC-2022-SYG Grant Agreement No 101071417 - RESILIENCE.

DATA AND CODE AVAILABILITY STATEMENT

All codes for numerical continuation and direct numerical simulation are provided in the Github repository `https://github.com/EntropicPhys/bwh_community`.

[1] J. M. Grünzweig and et al., "Dryland mechanisms could widely control ecosystem functioning in a drier and warmer world," Nature Ecology and Evolution **6**, 1064–1076 (2022).

[2] B. Zaitchik, M. Rodell, M. Biasutti, and et al., "Wetting and drying trends under climate change," Nat Water **1**, 502–513 (2023).

[3] A. K. Duraiappah and S. Naeem, "Ecosystems and human well-being: Biodiversity synthesis," Tech. Rep. of the Millennium Ecosystem Assessment (World Resources Institute, Washington, DC., 2005).

[4] F. T. Maestre, Y. L. Bagousse-Pinguet, M. Delgado-Baquerizo, D. J. Eldridge, H. Saiz, and et al., "Grazing and ecosystem service delivery in global drylands," Science **378**, 915–920 (2022).

[5] H. Heng Zhang, Y. Zhao, and J.-K. Zhu, "Thriving under stress: How plants balance growth and the stress response," Developmental Cell **55**, 529–543 (2020).

[6] M. Rietkerk and J. van de Koppel, "Regular pattern formation in real ecosystems," Trends in Ecology and evolution **23**, 169–175 (2008).

[7] E. Meron, "Vegetation pattern formation: The mechanisms behind the forms," Physics Today **72**, 30–36 (2019).

[8] G. Dovrat, E. Meron, M. Shachak, C. Golodets, and Y. Osem, "Plant size is related to biomass partitioning and stress resistance in water-limited annual plant communities," Journal of Arid Environments **165**, 1–9 (2019).

[9] B. K. Bera, O. Tzuk, J. J. R. Jamie JR Bennett, and E. Meron, "Linking spatial self-organization to community assembly and biodiversity," eLife **10**, e73819 (2021).

[10] A. J. Felton and M. D. Smith, "Integrating plant ecological responses to climate extremes from individual to ecosystem levels," Philosophical Transactions of the Royal Society B: Biological Sciences **372**, 20160142 (2017).

[11] S. E. Sultan, "Phenotypic plasticity for plant development, function and life history," trends in plant science **5**, 537–542 (2005).

[12] A. Daszkowska-Golec and I. Szarejko, "Open or close the gate - stomata action under the control of phytohormones in drought stress conditions," Front Plant Sci. **13**, 138 (2013).

[13] H. Fromm, "Root plasticity in the pursuit of water," Plants **8** (2019), 10.3390/plants8070236.

[14] M. Rietkerk, R. Bastiaansen, S. Banerjee, J. van de Koppel, M. Baudena, and A. Doelman, "Evasion of tipping in complex systems through spatial pattern formation," Science **374**, eabj0359 (2021).

[15] A. Bricca, M. D. Musciano, A. Ferrara, J.-P. Theurillat, and M. Cutini, "Community assembly along climatic gradient: Contrasting pattern between- and within- species," Perspectives in Plant Ecology, Evolution and Systematics **56**, 125675 (2022).

[16] C. Valentin, J. d'Herbes, and J. Poesen, "Soil and water components of banded vegetation patterns," Catena **37**, 1–24 (1999).

[17] V. Deblauwe, N. Barbier, P. Couteron, O. Lejeune, and J. Bogaert, "The global biogeography of semi-arid periodic vegetation patterns," Global Ecology and Biogeography **17**, 715–723 (2008).

[18] S. Getzin, H. Yizhaq, B. Bell, T. E. Erickson, A. C. Postle, I. Katra, O. Tzuk, Y. R. Zelnik, K. Wiegand, T. Wiegand, and E. Meron, "Discovery of fairy circles in australia supports self-organization theory," Proceedings of the National Academy of Sciences **113**, 3551–3556 (2016).

[19] J. J. R. Bennett, A. S. Gomes, M. A. Ferré, B. K. Bera, F. Borghetti, R. M. Callaway, and E. Meron, "Evidence for scale-dependent root-augmentation feedback and its role in halting the spread of a pantropical shrub into an endemic sedge," PNAS Nexus **2**, pgac294 (2023).

[20] J. J. R. Bennett, B. K. Bera, M. Ferré, H. Yizhaq, S. Getzin, and E. Meron, "Phenotypic plasticity: A missing element in the theory of vegetation pattern formation," Proceedings of the National Academy of Sciences **120**, e2311528120 (2023).

[21] C. Guill, J. Hülsemann, and T. Klauschies, "Self-organised pattern formation increases local diversity in metacommunities," Ecology Letters **24**, 2624–2634 (2021).

[22] K. Siteur, E. Siero, M. B. Eppinga, J. D. Rademacher, A. Doelman, and M. Rietkerk, "Beyond turing: The response of patterned ecosystems to environmental change," Ecological Complexity **20**, 81 – 96 (2014).

[23] R. Bastiaansen, O. Jaïbi, V. Deblauwe, M. B. Eppinga, K. Siteur, E. Siero, S. Mermoz, A. Bouvet, A. Doelman, and M. Rietkerk, "Multistability of model and real dryland ecosystems through spatial self-organization," Proceedings of the National Academy of Sciences **115**, 11256–11261 (2018).

[24] A. Asch, M. Avery, A. Cortez, and A. Scheel, "Slow passage through the busse balloon – predicting steps on the eckhaus staircase," European Journal of Applied Mathematics , 1–26 (2024).

[25] J. Nathan, Y. Osem, M. Shachak, and E. Meron, "Linking functional diversity to resource availability and disturbance: a mechanistic approach for water limited plant communities," Journal of Ecology **104**, 419–429 (2016).

[26] H. Yizhaq, M. Shachak, and E. Meron, "A model study of terraced riverbeds as novel ecosystems," Scientific Reports **10**, 3782 (2020).

[27] O. Tzuk, S. Ujjwal, C. Fernandez-Oto, M. Seifan, and E. Meron, "Period doubling as an indicator for ecosystem sensitivity to climate extremes," Scientific Reports **9**, 19577 (2019).

[28] H. Uecker, *Numerical continuation and bifurcation in Nonlinear PDEs* (SIAM, 2021).

[29] Z. Mei, *Numerical bifurcation analysis for reaction-diffusion equations*, Vol. 28 (Springer Science & Business Media, 2000).

[30] Y. R. Zelnik, E. Meron, and G. Bel, "Gradual regime shifts in fairy circles," Proceedings of the National Academy of Sciences **112**, 12327–12331 (2015).

[31] Y. R. Zelnik, S. Kinast, H. Yizhaq, G. Bel, and E. Meron, "Regime shifts in models of dryland vegetation," Philosophical Transactions R. Soc. A **371**, 20120358 (2013).

[32] S. van der Stelt, A. Doelman, G. M. Hek, and J. Rademacher, "Rise and fall of periodic patterns for a generalized klausmeier-gray-scott model," J. Nonlinear Sci. **23**, 39 – 95 (2013).

[33] E. Knobloch, "Spatial localization in dissipative systems," Annual Review of Condensed Matter Physics **6**, 325–359 (2015).

[34] E. Meron, *Nonlinear Physics of Ecosystems* (CRC Press, Taylor & Francis Group, 2015).

[35] E. Meron, "From patterns to function in living systems: Dryland ecosystems as a case study," Annual Review of Condensed Matter Physics **9**, 79–103 (2018).

[36] S. Kinast, Y. R. Zelnik, G. Bel, and E. Meron, "Interplay between turing mechanisms can increase pattern diversity," Phys. Rev. Lett. **112**, 078701 (2014).

[37] F. Tardieu, "Any trait or trait-related allele can confer drought tolerance: just design the right drought scenario," Journal of Experimental Botany **63**, 25–31 (2011).

[38] R. Croce, E. Carmo-Silva, Y. B. Cho, M. Ermakova, J. Harbinson, T. Lawson, A. J. McCormick, K. K. Niyogi, D. R. Ort, D. Patel-Tupper, P. Pesaresi, C. Raines, A. P. M. Weber, and X.-G. Zhu, "Perspectives on improving photosynthesis to increase crop yield," The Plant Cell , koae132 (2024).

[39] Y. R. Zelnik, Y. Mau, M. Shachak, and E. Meron, "High-integrity human intervention in ecosystems: Tracking self-organization modes," PLOS Computational Biology **17**, 1–23 (2021).